Mouse MRI: Concepts and Applications in Physiology

Robia G. Pautler

EMERGING TECHNOLOGIES

Mouse MRI: Concepts and Applications in Physiology

Robia G. Pautler

Department of Molecular Physiology and Biophysics, Baylor
College of Medicine, Houston, Texas 77030
rpautler@bcm.tmc.edu

The purpose of this review is to provide an introduction to the rapidly expanding field of mouse magnetic resonance imaging (MRI). It is by no means meant to be all-inclusive but rather to provide a brief introduction to the basics of MRI theory, provide some insight into the basic experiments that can be performed in mice by using MRI, and bring to light some factors to consider when planning a mouse MRI experiment.

In the biological sciences, many studies using mouse models are limited by the inability to gather anatomical and physiological information noninvasively in a longitudinal manner. Invasive imaging modalities such as 2-photon microscopy that provide images of a very high spatial resolution are limited by a depth resolution of a few hundred microns into the mouse. Clearly, there is a great need in mouse research for imaging modalities that can provide in vivo, noninvasive anatomical and physiological information that can be collected in three dimensions at a high spatial and temporal resolution.

Magnetic resonance imaging (MRI) is a very attractive noninvasive imaging modality because it does not rely on ionizing radiation and offers a spatial resolution of tens of microns, exhibiting clear advantages over other imaging methodologies such as positron emission tomography (PET) or X-rays. Additionally, images can be acquired relatively quickly. Compared with traditional histological techniques, which are quite time consuming (taking several days to weeks), MRI images can be acquired in three-dimensional data sets with a very accurate depiction of a sample in a relatively short amount of time (a few hours). Most importantly, images can be acquired in vivo, allowing for the longitudinal acquisition of anatomical and physiological information from the same subject.

With the advent of stronger magnetic fields that allow for better signal-to-noise ratios in MRI images as well as the development of stronger gradients that currently push the spatial resolution of MRI images to that of 10–50 μm, it is clear that MRI technology has advanced to a level that is now capable of providing insights into mouse phenotyping that have not been previously possible.

Most of the MRI imaging that occurs in biological research is centered on signal from hydrogen (^{1}H) because of its proportionally large natural abundance in biological systems as well as the associated large magnetic moment (4, 25). To understand where the signal in ^{1}H-MRI comes from, the basic anatomy of the atom needs to be revisited.

An atom consists of a nucleus that is surrounded by orbiting electrons. Within the nucleus of a hydrogen atom is a positively charged proton. In addition to having a positive charge, it is important to note that protons are also spinning. According to the fundamental principles of electromagnetism, a charged particle that is moving induces a magnetic field. Hence, it is perhaps easiest to conceptualize these protons as tiny magnets or "spins" (4, 25).

In a sample containing hydrogen located on the laboratory benchtop, the orientation of the spins will be random (FIGURE 1A, step 1). However, when the same sample is placed in an external magnetic field (B_0), a small excess of the spins will align with B_0 (FIGURE 1A, step 2). The spins aligned in the same direction as B_0 will combine, resulting in a net magnetization vector (NMV) that precesses around B_0 at a specified frequency, ω (FIGURE 1A, steps 3 and 4). This plane is referred to as the longitudinal plane (4, 25).

Associated with the MRI nuclei of interest (in this case the proton) is a constant known as the gyromagnetic ratio (γ) that is directly proportional to the precessional frequency. The γ for hydrogen is 42.58 MHz/T, and typical values for B_0 range from 1.5 T to as high as 14 T.[*] The precessional frequency, ω, is represented by the Larmour equation:

$$\omega = \gamma B_0$$

Protons precess at a frequency that falls into the radio frequency (RF) range. If an RF pulse is applied to this precessing NMV and at 90° to the NMV, the NMV will absorb energy, change direction, and subsequently precess in the transverse plane (FIGURE 1A, step 5). For the duration of the RF pulse, the NMV will remain in the transverse plane (4, 25). The application of an RF pulse is known as "excitation."

Once the pulse is turned off, the NMV will recover or "relax" back to the longitudinal plane and once again precess around the main magnetic field. This recovery process along the longitudinal plane is known as spin-lattice relaxation (T_1), and the decay along the transverse plane is known as spin-spin relaxation (T_2) (FIGURE 1A, step 6). T_1 recovery is due to nuclei giving up energy to the surrounding environment, whereas T_2 decay is due to nuclei exchanging energy with other nuclei (4, 25).

[*]As B_0 increases, the signal-to-noise ratio will improve. For mouse MRI imaging, it is best to minimally have a B_0 of at least 4.7 T and preferably at least 7.0 T. Incidentally, horizontal scanners are preferable to vertical scanners for the obvious reason that it is easier to lay the animal prone rather than have it suspended by its teeth.
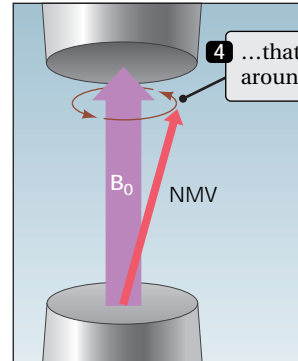
EMERGING TECHNOLOGIES

A

1 Protons—positively charged particles—spin in random directions in the absence of an external magnetic field.
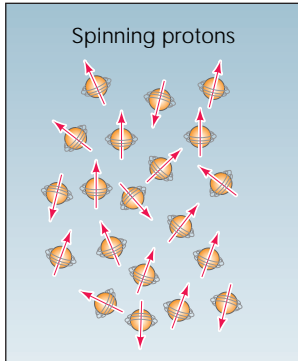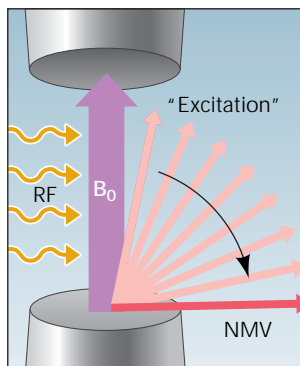
2 If a magnetic field, B_0, is applied, a small proportion of the spinning protons (which are like tiny magnets) tend to align with it.
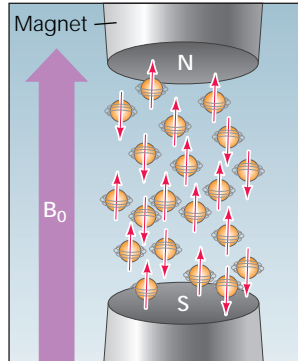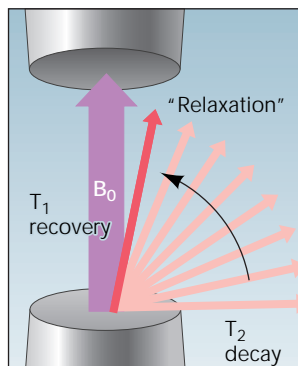
3 If the spins aligned with B_0 are added together, they result in a net magnetization vector (NMV)…

Spinning protons

Magnet

N

4 …that precesses around B_0.

B_0

B_0 NMV

B_0

S

B

"Excitation"

RF B_0

NMV

"Relaxation"

T_1 recovery B_0
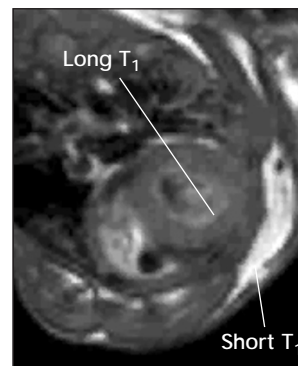
T_2 decay

Long T_1

Short T_1

5 Applying a radio frequency (RF) at 90° ("excitation") causes the NMV to move from the longitudinal to the transverse plane.

6 When the RF is turned off, the transverse component (T_2) decays and the longitudinal component (T_1) recovers.

Contrast arises because different tissues have different decay are recovery times (T_2 and T_1 values).

FIGURE 1. Basic description of magnetic resonance imaging (MRI)
A: steps in the MRI process. *B*: contrast arising from different T_1 and T_2 values. In a T_1-weighted MRI image, tissues with a shorter T_1 will have a higher signal intensity than tissues with a longer T_1. T_1-weighted contrast agents such as Gd-DTPA or Mn^{2+} shorten the T_1 of tissue H_2O, resulting in an increase in signal intensity in the tissues where the contrast agent has accumulated. Adapted from Ref. 25.

A receiver coil placed in the transverse plane can detect the NMV. When the coherent NMV in the transverse plane cuts across this coil, a voltage is induced in the coil. This is the MRI signal. The timing between RF pulses is known as the repetition time (TR), and the timing from the RF pulse to the acquisition of the signal induced in the coil is known as the echo time (TE) (4, 25).

If the NMV of every tissue type recovered to the original position around B_0 at the same rate, it would be impossible to discern the contrast between the different tissue types, because all tissues would consequently have uniform signal intensity. Contrast in MRI images arises from the fact that different tissue types can relax at different rates (i.e., have different T_1 and T_2 values) (FIGURE 1B). The standard and easiest example is to compare fat and water. Fat is quite simply comprised of hydrogen and carbon, whereas water is made up of hydrogen bonded to oxygen. Fat has a very slow molecular tumbling relative to water that causes the recovery of the NMV to be faster (short T_1), whereas water has a high molecular mobility that yields a less-efficient recovery of the NMV (long T_1) (4, 25).

In addition to inherent tissue contrast, there are exogenous agents that can be applied to tissues or organ systems that cause significant alterations in the local T_1 and/or T_2 that ultimately result in an alteration of the local magnetic field. These agents are called MRI contrast agents and, depending on the type of agent used, can cause either positive (increased signal intensity) or negative (decreased signal intensity) contrast enhancement in MRI images of tissues or organs where the agent has accumulated (4, 25). Some examples of MRI contrast agents include chelated gadolinium (Gd^{3+}), manganese (Mn^{2+}), and iron (Fe^{3+}).

Basic mouse MRI experiments

There are three basic types of mouse MRI experiments. These include anatomical and dynamic MRI acquisitions in addition to a specialized field of MRI imaging known as molecular imaging. Some examples of these different types of imaging are summarized in TABLE 1.

EMERGING TECHNOLOGIES

TABLE 1. Some different types of experiments that can be performed using MRI

Organ/Structure of Interest	Imaging Modality	Type of Information
Brain	T_1-weighted MRI, spin echo (TR = 500 ms, FOV = 1.5 cm, phase encodes = 128, TE = 7 ms, no. of slices = 128)	Anatomy; very little differentiation between gray and white matter in mouse; useful for incorporating T_1-weighted contrast agents; also useful for assessing fat content
	T_2-weighted MRI, spin echo (TR = 1,275 ms, FOV = 1.5 cm, phase encodes = 128, TE = 25 ms, no. of slices = 128)	Anatomy, good differentiation between gray and white matter in mouse, excellent in rat
	T_1-weighted MRI, spin echo (TR = 500 ms, FOV = 1.5 cm, phase encodes = 256, no. of slices = 256)	Anatomy; very little differentiation between gray and white matter in mouse; useful for incorporating T_1-weighted contrast agents; also useful for assessing fat content
	T_2-weighted MRI, spin echo (TR = 1,275 ms, FOV = 1.5 cm, phase encodes = 256, no. of slices = 256)	Anatomy, good differentiation between gray and white matter in mouse, excellent in rat
	BOLD	Monitoring of changes in blood flow, reflective of neuronal activation local field potentials but not spiking activity; used in rat models, not yet readily used in mouse models
	Diffusion tensor imaging	Orientation of white matter tracts
	MEMRI T_1-weighted MRI, spin echo (TR = 500 ms, FOV = 1.5–3.0 cm, phase encodes = 128, no. of slices = 128)	Anatomical tract tracings from the mouse olfactory and visual systems; tracings from the striatum and amygdala; activity-dependent tracings in the olfactory system; information on anatomical connectivity and enhancement of specific brain nuclei
	T_1 measure (inversion recovery)	Measure T_1 and changes in T_1 based on tissue type or disease state
	T_2 measure (spin echo)	Measure T_2 and changes in T_2 based on tissue type or disease state
Heart	FLASH imaging	Velocity, magnitude, and direction of the myocardium left ventricular volume Coronary artery and heart valve structure
	MEMRI T_1-weighted MRI, FLASH (TR = 300 ms, FOV = 2.5 cm)	Calcium influx and inotropy
Lungs	Short TE gradient echo sequence	T_2^* relaxation times
	Proton density-weighted imaging	Lung parenchyma, lung volume, and lung tumor assessment
Kidney	T_1-weighted MRI in conjunction with pH-sensitive contrast agents	Measurement of pH
	3-D MRI	Examination of polycystic kidney disease
	Dynamic contrast-enhanced MRI	Renal tube damage
Tumors	T_1- and T_2-weighted dynamic, contrast-enhanced MRI using chelated gadolinium	Highlight tumors to monitor size and growth; examination of tumor angiogenesis

MRI, magnetic resonance imaging; T_1, spin-lattice relaxation; T_2, spin-spin relaxation; T_2^*, apparant T_2, which takes into account the influence   of n
enhanced MRI; FLASH, fast low-angle shot; TE, echo time; 3-D, three-dimensional.

Spatial Resolution	Acquisition Time	Analysis	References
117 μm	A few minutes for a single slice, 2.27 h for 128 slices (3-D intensity volume)	Segmentation, measurement of signal intensity	5, 18, 31, 32
117 μm	A few minutes for a single slice, 5.80 h for 128 slices (3-D intensity volume)	Segmentation, measurement of signal intensity	
58.5 μm	Tens of minutes for a single slice 9 h for 128 slices (3-D volume)	Segmentation, measurement of signal intensity	
58.5 μm	1.5 h for a single slice 23.2 h for 256 slices (3-D volume)	Segmentation, measurement of signal intensity	
180 μm 469 μm	11 s/slice	AFNI and cross-correlation test t-test	1, 11
~40 μm	24 h	Calculation of diffusion tensor and color maps	29
117–234 μm	~3 h	Measurement of signal intensity	13–15
~200 μm	Tens of minutes	Measurement of T_1 and signal intensity	9, 18, 29
~200 μm	Tens of minutes	Measurement of T_2 and signal intensity	
~200 μm 100 μm	10 ms	Segmentation	10, 17, 20
195 μm	40–60 min for the entire time course	Measurement of signal intensity	10
400–740 μm	89 s	3-D volume rendering, color segmentation	2, 3
		Measurement of signal intensity	
		MRI pH map	16, 22
	1 h total imaging time	Segmentation, volume calculation	
160 μm		Dynamics of contrast enhancement	
100–400 μm	Tens of minutes to several hours	Measurement of signal intensity; characterization of blood vessels	2, 6, 7, 8, 23

ence   of magnetic field inhomogeneities on T_2; TR, repetition time; FOV, field of view; BOLD, blood oxygen level detection; MEMRI, manganese-
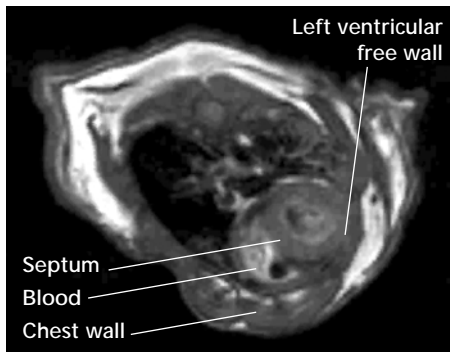
EMERGING TECHNOLOGIES

FIGURE 2. **Anatomical image of the mouse heart from a fast spin-echo imaging sequence**
This image was cardiac and respiratory gated to minimize artifacts due to the motion of the beating heart as well as respiration and was acquired on an 11.7 T Bruker Avance system.

Anatomical MRI image acquisitions are relatively straightforward in that high-resolution scans can be acquired to determine the volume or surface area of a specific tissue or organ or the orientation of fibers within an organ (FIGURE 2). The typical anatomical MRI experiment consists of selecting the imaging sequence and parameters that will provide optimal signal intensity and contrast within the tissues/organs of interest, acquiring the MRI data, and then using postprocessing software to measure signal intensities or color segment regions of interest and to calculate surface areas or volumes.

Additionally, the T_1 and T_2 of the tissues can be measured, because these values can change during a disease state (5, 18). These two measurements are acquired separately. Typically, an "inversion recovery sequence" is chosen to measure the T_1 with a long TR and varying inversion times (TI) (4, 25). For measuring T_2, a series of images is acquired with a long TR and a varying TE (4, 25).

After the data are collected, either a T_1 or T_2 map can be generated that gives a color-coded representation of the varying T_1 or T_2 values within the tissue/organ of interest.

Some examples of anatomical mouse MRI imaging include the determination of tissue/organ or tumor sizes and monitoring changes over time. For example, Susumu Mori's group (30) has elegantly monitored central nervous system changes by using MRI in the developing mouse embryo. Additional uses of anatomical mouse MRI include mapping neuronal connections by measuring the diffusion of water along axonal pathways, detecting atherosclerotic plaque in major vessels, and discovering changes in T_2 due to neuritic plaque formation in mouse models of Alzheimer's disease (22, 27, 31).

Dynamic MRI experiments, as the name implies, involve the monitoring of a structure over time and determining any ensuing changes that occur during this time course. Dynamic MRI can entail the monitoring of the nor-

mal activity of a system or can monitor anatomical and physiological changes in response to a stimuli or disease state.

Perhaps one of the best-known forms of dynamic MRI experiments is that of functional MRI (fMRI). fMRI typically refers to the monitoring of changes in blood flow. Quite commonly, blood oxygen level detection (BOLD) imaging is used in fMRI studies (4). Increased blood flow has been correlated with increases in neuronal activation, reflective of local field potentials (4, 19). BOLD relies on changes in blood flow, blood volume, and the oxygenation state of blood to alter the MRI signal (4). Fast imaging sequences such as echo-planar imaging (EPI) or fast gradient echo imaging sequences are used in BOLD fMRI studies (4).

Additionally, fast imaging sequences can be used in dynamic MRI studies to monitor the inflow or uptake of contrast agents. For example, contrast agents can be used to determine changes in vascular permeability of tumors, providing an assessment of the first-pass dynamics of the agent to assess muscle injury, determine renal perfusion and function, etc. (FIGURE 3) (12, 23, 28). Furthermore, organs that exhibit a lot of movement such as the heart or the gastrointestinal tract can be imaged by using fast imaging sequences [e.g., fast low-angle shot (FLASH) or ultrafast, low-angle, rapid acquisition and relaxation enhancement (UFLARE)] and can offer infor-

FIGURE 3. **MRI in a severe combined immunodeficiency mouse bearing an orthotopic human pancreatic tumor (arrows) 15 days after injection of CAPAN-2 cells into the tail of the pancreas**
T_1-weighted images without Gd-DTPA (T_1 contrast agent) (A) and with Gd-DTPA (B and C) are shown. Note that the kidneys also exhibit enhancement due to the processing of the contrast agent for excretion. Adapted from Grimm et al., *Int J Cancer*, Copyright 2003 John Wiley & Sons (7).
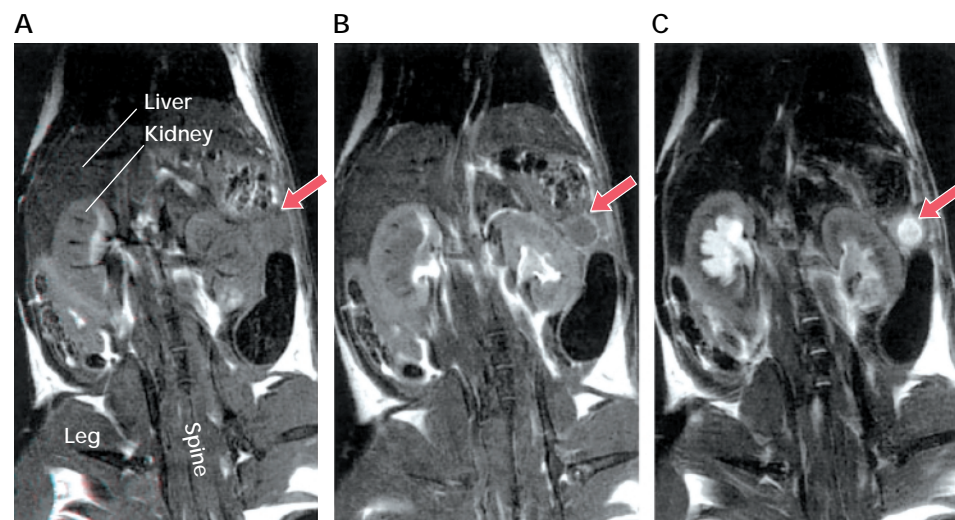
FIGURE 4. MRI detection of Alzheimer's disease plaques by using an engineered contrast agent
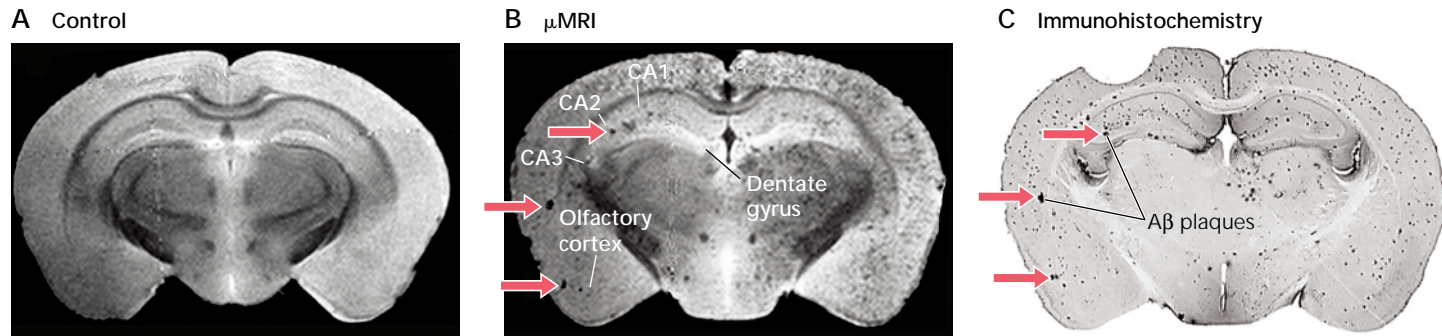Aβ plaques were detected with ex vivo μMRI after injection of Gd-DTPA-Aβ 1−40 with mannitol. A 6-mo-old control mouse (A) and APP/PS1-transgenic mouse (B) are shown. Both brains were extracted and prepared for imaging 6 h after carotid injection of Gd-DTPA-Aβ 1−40 with 15% mannitol. Note the obvious matching of many larger plaques (arrows) between μMRI (B) and immunohistochemistry (C). Adapted from Ref. 24.

mation such as blood flow dynamics, calcium influx, ventricular volumes throughout the cardiac cycle, contractility, gut motility, or bolus volume (10, 26). Gating the image acquisition to the cardiac or respiratory cycle contributes significantly toward the reduction of motion artifacts within the image.

Molecular imaging is an emerging field of MRI imaging that oftentimes uses engineered contrast agents to monitor changes in anatomy or physiology. Additionally, the magnetic labeling of transplanted cells to monitor the progression of cell mobilization falls into this category. The field is rapidly expanding and is making progress as a robust field of study. Some examples of molecular imaging include monitoring apoptosis by magnetically labeling the C2 domain of synaptotagmin I, which binds to plasma membranes of apoptotic cells (32). Additionally, Wadghiri et al. (24) have magnetically labeled the Aβ 1−40 peptide that is known to bind to amyloid precursor protein (APP) and have been able to discern AD plaques in transgenic mice overexpressing APP (FIGURE 4). Some general issues with engineered contrast agents, however, are being able to target the agent, obtaining enough contrast from the agent, toxicity issues, and being able to turn the agent "on/off."

Conclusion

The future of MRI in biomedical research will depend on providing current and future investigators with a basic foundation in MRI and will bring to light factors to consider when planning a mouse MRI experiment, thereby allowing this imaging modality to be used as a tool to help accelerate the analysis and understanding of the vast, growing number of mouse models of disease and behaviors (TABLE 2; see next page). MRI has rapidly evolved, and the time is suitable to bridge the gap between the existing technology and hypothesis-driven applications in murine-based biomedical research. ■
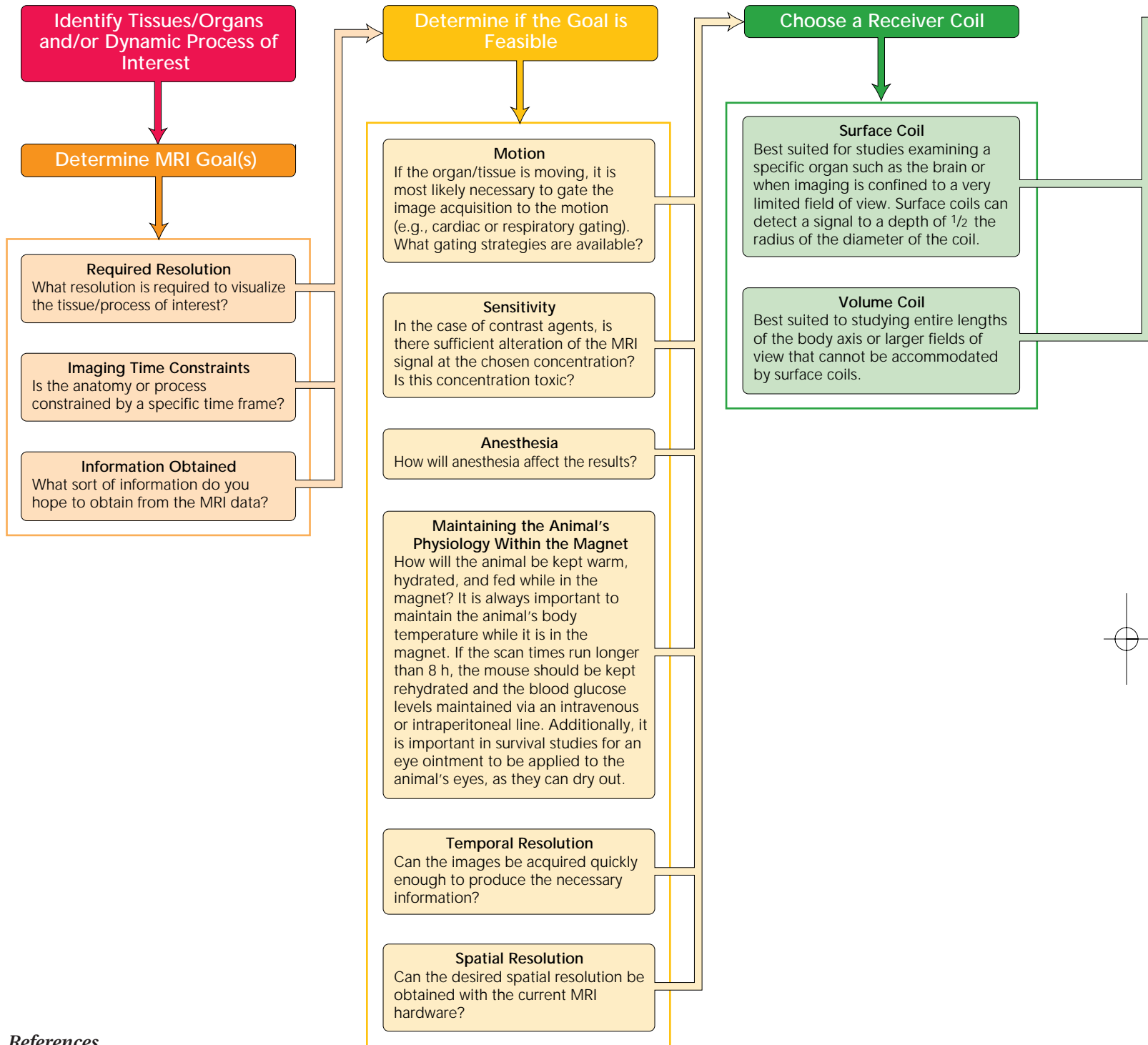
"If you can learn to run a microscope, then you most certainly can learn to run a magnet."
– Alan Koretsky, Ph.D., personal communication to Robia G. Pautler, first year graduate school, Carnegie Mellon University, 1994
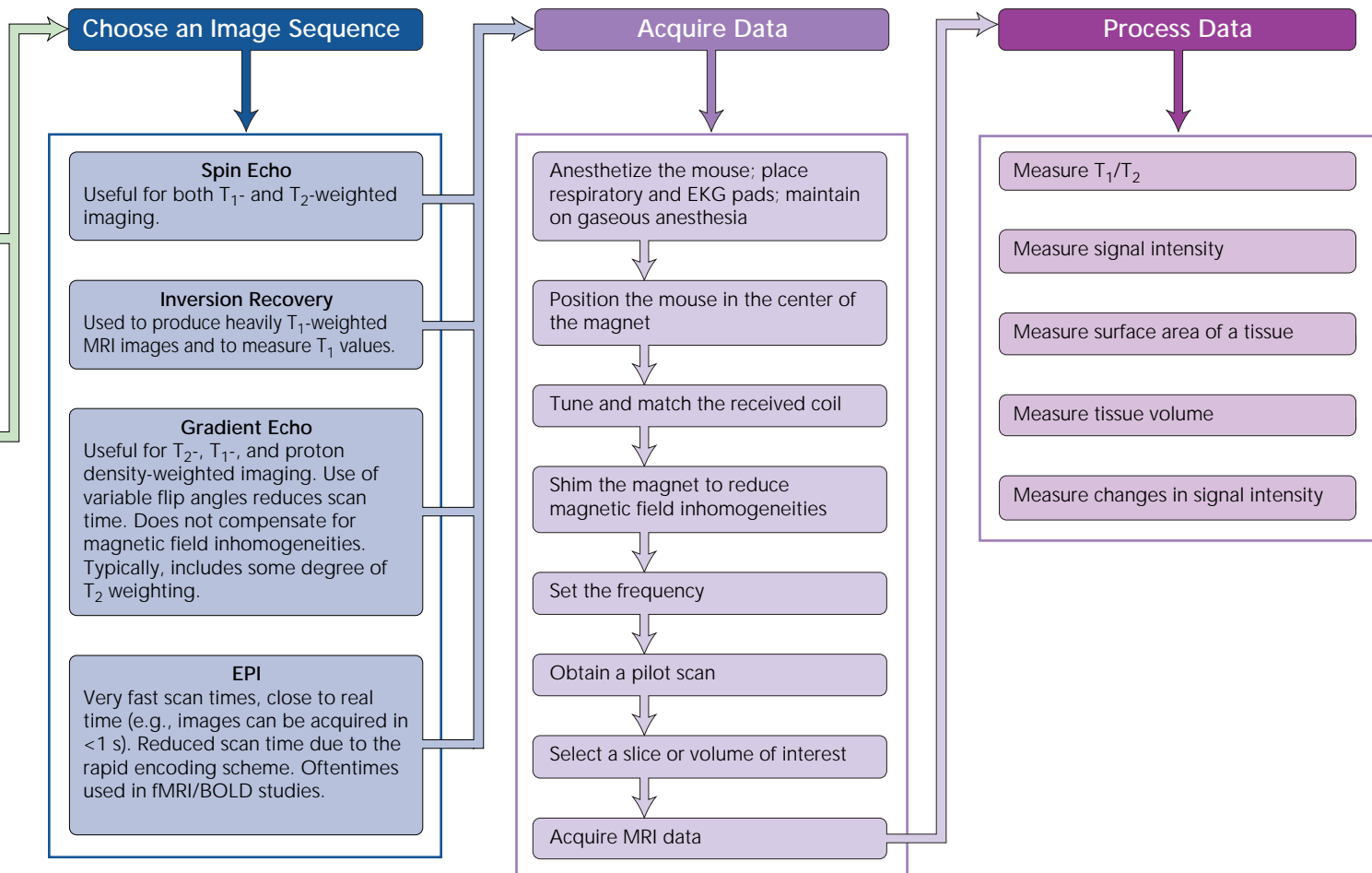
EMERGING TECHNOLOGIES

TABLE 2. General outline for planning a mouse MRI experiment, including some sample imaging sequences

```
┌─────────────────────────┐       ┌─────────────────────────┐       ┌─────────────────────────┐
│ Identify Tissues/Organs │       │ Determine if the Goal is│       │  Choose a Receiver Coil │
│ and/or Dynamic Process  │  ──▶  │         Feasible        │  ──▶  │                         │
│        of Interest      │       └─────────────────────────┘       └─────────────────────────┘
└─────────────────────────┘
```

Identify Tissues/Organs and/or Dynamic Process of Interest

Determine MRI Goal(s)

Required Resolution
What resolution is required to visualize the tissue/process of interest?

Imaging Time Constraints
Is the anatomy or process constrained by a specific time frame?

Information Obtained
What sort of information do you hope to obtain from the MRI data?

Determine if the Goal is Feasible

Motion
If the organ/tissue is moving, it is most likely necessary to gate the image acquisition to the motion (e.g., cardiac or respiratory gating). What gating strategies are available?

Sensitivity
In the case of contrast agents, is there sufficient alteration of the MRI signal at the chosen concentration? Is this concentration toxic?

Anesthesia
How will anesthesia affect the results?

Maintaining the Animal's Physiology Within the Magnet
How will the animal be kept warm, hydrated, and fed while in the magnet? It is always important to maintain the animal's body temperature while it is in the magnet. If the scan times run longer than 8 h, the mouse should be kept rehydrated and the blood glucose levels maintained via an intravenous or intraperitoneal line. Additionally, it is important in survival studies for an eye ointment to be applied to the animal's eyes, as they can dry out.

Temporal Resolution
Can the images be acquired quickly enough to produce the necessary information?

Spatial Resolution
Can the desired spatial resolution be obtained with the current MRI hardware?

Choose a Receiver Coil

Surface Coil
Best suited for studies examining a specific organ such as the brain or when imaging is confined to a very limited field of view. Surface coils can detect a signal to a depth of $\frac{1}{2}$ the radius of the diameter of the coil.

Volume Coil
Best suited to studying entire lengths of the body axis or larger fields of view that cannot be accommodated by surface coils.

References

1. Ahrens ET and Dubowitz DJ. Peripheral somatosensory fMRI in mouse at 11.7 T. *NMR Biomed* 14: 318–324, 2001.

2. Asanuma T, Ohkura K, Yamamoto T, Kon Y, Shimokawa S, and Kuwabara M. Three-dimensional magnetic resonance imaging of lung and liver tumors in mice by use of transversal multi-slice magnetic resonance images. *Comp Med* 51: 138–144, 2001.

3. Beckmann N, Tigani B, Mazzoni L, and Fozard JR. MRI of lung parenchyma in rats and mice using a gradient-echo sequence. *NMR Biomed* 14: 297–306, 2001.

4. Buxton R. *Introduction to Functional Magnetic Resonance Imaging: Principles and Techniques.* New York: Cambridge University Press, 2001.

5. Dunn JF and Zaim-Wadghiri Y. Quantitative magnetic resonance imaging of the mdx mouse model of Duchenne muscular dystrophy. *Muscle Nerve* 22: 1367–1371. 1999.

6. Fink C, Kiessling F, Bock M, Lichy MP, Misselwitz B, Peschke P, Fusenig NE, Grobholz R, and Delorme S. High-resolution three-dimensional M.R. angiography of rodent tumors: morphologic characterization of intratumoral vasculature. *J Magn Reson Imaging* 18: 59–65, 2003.

7. Grimm J, Potthast A, Wunder A, and Moore A. Magnetic resonance imaging of the pancreas and pancreatic tumors in a mouse orthotopic model of human cancer. *Int J Cancer* 106: 806–811, 2003.

8. Guccione S, Yang YS, Shi G, Lee DY, Li KC, and Bednarski MD. Functional genomics guided with M.R. imaging: mouse tumor model study. *Radiology* 228: 560–568, 2003.

9. Guilfoyle DN, Dyakin VV, O'Shea J, Pell GS, and Helpern JA. Quantitative measurements of proton spin-lattice (T1) and spin-spin (T2) relaxation times in the mouse brain at 70 T. *Magn Reson Med* 49: 576–580, 2003.

Choose an Image Sequence

Spin Echo
Useful for both T_1- and T_2-weighted imaging.

Inversion Recovery
Used to produce heavily T_1-weighted MRI images and to measure T_1 values.

Gradient Echo
Useful for T_2-, T_1-, and proton density-weighted imaging. Use of variable flip angles reduces scan time. Does not compensate for magnetic field inhomogeneities. Typically, includes some degree of T_2 weighting.

EPI
Very fast scan times, close to real time (e.g., images can be acquired in <1 s). Reduced scan time due to the rapid encoding scheme. Oftentimes used in fMRI/BOLD studies.

Acquire Data

Anesthetize the mouse; place respiratory and EKG pads; maintain on gaseous anesthesia

Position the mouse in the center of the magnet

Tune and match the received coil

Shim the magnet to reduce magnetic field inhomogeneities

Set the frequency

Obtain a pilot scan

Select a slice or volume of interest

Acquire MRI data

Process Data

Measure T_1/T_2

Measure signal intensity

Measure surface area of a tissue

Measure tissue volume

Measure changes in signal intensity

10. Hu TC, Pautler RG, MacGowan GA, and Koretsky AP. Manganese-enhanced MRI of mouse heart during changes in inotropy. *Magn Reson Med* 46: 884–890, 2001.

11. Kennan RP, Suzuka SM, Nagel RL, and Fabry ME. Decreased cerebral perfusion correlates with increased BOLD hyperoxia response in transgenic mouse models of sickle cell disease. *Magn Reson Med* 51: 525–532, 2004.

12. Kobayashi H, Kawamoto S, Jo SK, Sato N, Saga T, Hiraga A, Konishi J, Hu S, Togashi K, Brechbiel MW, and Star RA. Renal tubular damage detected by dynamic micro-MRI with a dendrimer-based magnetic resonance contrast agent. *Kidney Int* 61: 1980–1985, 2002.

13. Pautler RG and Koretsky AP. Tracing odor-induced activation in the olfactory bulbs of mice using manganese-enhanced magnetic resonance imaging. *Neuroimage* 16: 441–448, 2002.

14. Pautler RG, Mongeau R, and Jacobs RE. In vivo trans-synaptic tract tracing from the murine striatum and amygdala utilizing manganese enhanced MRI (MEMRI). *Magn Reson Med* 50: 33–39, 2003.

15. Pautler RG, Silva AC, and Koretsky AP. In vivo neuronal tract tracing using manganese-enhanced magnetic resonance imaging. *Magn Reson Med* 40: 740–748, 1998.

16. Raghunand N, Howison C, Sherry AD, Zhang S, and Gillies RJ. Renal and systemic pH imaging by contrast-enhanced MRI. *Magn Reson Med* 49: 249–257, 2003.

17. Ruff J, Wiesmann F, Lanz T, and Haase A. Magnetic resonance imaging of coronary arteries and heart valves in a living mouse: techniques and preliminary results. *J Magn Reson* 146: 290–296, 2000.

18. Sadowski M, Tang CY, Aguinaldo JG, Carp R, Meeker HC, and Wisniewski T. In vivo micro magnetic resonance imaging signal changes in scrapie infected mice. *Neurosci Lett* 345: 1–4, 2003.

19. Saleem KS, Pauls JM, Augath M, Trinath T, Prause BA, Hashikawa T, and Logothetis NK. Magnetic resonance imaging of neuronal connections in the macaque monkey. *Neuron* 34: 685–700, 2002.

20. Streif JU, Herold V, Szimtenings M, Lanz TE, Nahrendorf M, Wiesmann F, Rommel E, and Haase A. In vivo time-resolved quantitative motion mapping of the murine myocardium with phase contrast MRI. *Magn Reson Med* 49: 315–321, 2003.

21. Sun SW, Neil JJ, and Song SK. Relative indices of water diffusion anisotropy are equivalent in live and formalin-fixed mouse brains. *Magn Reson Med* 50: 743–748, 2003.

22. Sun Y, Zhou J, Stayner C, Munasinghe J, Shen X, Beier DR, and Albert MS. Magnetic resonance imaging assessment of a murine model of recessive polycystic kidney disease. *Comp Med* 52: 433–438, 2002.

23. Tailor DR, Poptani H, Glickson JD, Leigh JS, and Reddy R. High-resolution assessment of blood flow in murine RIF-1 tumors by monitoring uptake of $H_2$¹⁷O with proton T(1rho)-weighted imaging. *Magn Reson Med* 49: 1–6, 2003.

24. Wadghiri YZ, Sigurdsson EM, Sadowski M, Elliott JI, Li Y, Scholtzova H, Tang CY, Aguinaldo G, Pappolla M, Duff K, Wisniewski T, and Turnbull DH. Detection of Alzheimer's amyloid in transgenic mice using magnetic resonance microimaging. *Magn Reson Med* 50: 293–302, 2003.

25. Westbrook C and Kaut Roth C. *MRI in Practice* (2nd ed.). Oxford, UK: Blackwell, 1998.

26. Wiesmann F, Ruff J, Engelhardt S, Hein L, Dienesch C, Leupold A, Illinger R, Frydrychowicz A, Hiller KH, Rommel E, Haase A, Lohse MJ, and Neubauer S. Dobutamine-stress magnetic resonance microimaging in mice: acute changes of cardiac geometry and function in normal and failing murine hearts. *Circ Res* 88: 563–569, 2001.

27. Wiesmann F, Szimtenings M, Frydrychowicz A, Illinger R, Hunecke A, Rommel E, Neubauer S, and Haase A. High-resolution MRI with cardiac and respiratory gating allows for accurate in vivo atherosclerotic plaque visualization in the murine aortic arch. *Magn Reson Med* 50: 69–74, 2003.

28. Wishnia A, Alameddine H, Tardif de Gery S, and Leroy-Willig A. Use of magnetic resonance imaging for noninvasive characterization and follow-up of an experimental injury to normal mouse muscles. *Neuromuscul Disord* 11: 50–55, 2001.

29. Zhang J, Richards LJ, Yarowsky P, Huang H, van Zijl PC, and Mori S. Three-dimensional anatomical characterization of the developing mouse brain by diffusion tensor microimaging. *Neuroimage* 20: 1639–1648, 2003.

30. Zhang J, van Zijl PC, and Mori S. Three-dimensional diffusion tensor magnetic resonance microimaging of adult mouse brain, and hippocampus. *Neuroimage* 15: 892–901, 2002.

31. Zhang J, Yarowsky P, Gordon MN, Di Carlo G, Munireddy S, van Zijl PC, and Mori S. Detection of amyloid plaques in mouse models of Alzheimer's disease by magnetic resonance imaging. *Magn Reson Med* 51: 452–457, 2004.

32. Zhao M, Beauregard DA, Loizou L, Davletov B, and Brindle KM. Non-invasive detection of apoptosis using magnetic resonance imaging and a targeted contrast agent. *Nat Med* 7: 1241–1244, 2001.